Arabian Journal of Chemistry (2020) 13, 8262–8270

King Saud University

Arabian Journal of Chemistry

www.ksu.edu.sa
www.sciencedirect.com

ORIGINAL ARTICLE

Multifunctional $Zn_{0.3}Al_{0.4}O_{4.5}$ crystals: An efficient photocatalyst for formaldehyde degradation and EBT adsorption

Umesh Fegade [a,*], Ganesh Jethave [b], Wei-Gang Hong [c], Imran Khan [d], Hadi M. Marwani [e], Inamuddin [e,*], Ren-Jang Wu [c,], Rajesh Dhake [f]**

[a] *Department of Chemistry, Bhusawal Arts, Science and P.O. Nahata Commerce College, Bhusawal, Jalgaon 425201 (M.H.), India*
[b] *School of Environmental and Earth Sciences, Kavayitri Bahinabai Chaudhari North Maharashtra University, Jalgaon 425001 (M.H.), India*
[c] *Department of Applied Chemistry, Providence University, Shalu, Taichung 433, Taiwan*
[d] *Applied Science Section, Faculty of Engineering and Technology, Aligarh Muslim University, Aligarh 202 002, India*
[e] *Chemistry Department, Faculty of Science, King Abdulaziz University, Jeddah 21589, Saudi Arabia*
[f] *Department of Chemistry, D. D. N. Bhole College, Bhusawal, Jalgaon 25201 (M.H.), India*

Received 10 March 2020; accepted 2 April 2020
Available online 10 April 2020

KEYWORDS

ZnAlONPs;
HCHO degradation;
Eriochrome black T;
Pseudo second order model;
Langmuir isotherm

Abstract The $Zn_{0.3}Al_{0.4}O_{4.5}$ nanoparticles (ZnAlONPs) with size of 70–90 nm are used as an efficient photocatalyst for formaldehyde (HCHO) degradation and effective adsorbent for the removal of eriochrome black-T (EBT) dye from synthetic aqueous solution. Degradation of HCHO reactions were studied using TiO_2 (homemade), TiO_2 (P-25) and ZnAlONPs by irradiating under 18 W daylight lamp source for photocatalytic degradation. The HCHO degradation rate is about 67, 76 and 89% for TiO_2 (homemade), TiO_2 (P25) and ZnAlONPs during 2 h reaction, respectively at initial formaldehyde gas concentration of 20 ppm. Maximum adsorption capacity was optimized by changing the parameters such as pH, EBT concentration and adsorbent dosage. A 200 mg of ZnAlONPs are useable for quick removal of EBT (>95%). Langmuir isotherm model showed a maximum adsorption capacity of 90.90 mgg^{-1}. The ZnAlONPs could be successfully reused upto 5^{th} adsorption/desorption cycle for EBT dye removal from water samples.

** Corresponding author.
E-mail addresses: umeshfegade@gmail.com (U. Fegade), inamuddin@zhcet.ac.in (Inamuddin), rjwu@pu.edu.tw (R.-J. Wu).
Peer review under responsibility of King Saud University.

ELSEVIER Production and hosting by Elsevier

1. Introduction

Environmental pollution originated by HCHO, is becoming a severe problem in front of scientists and researchers. Among the many chemical contaminants usually found in polluted indoor air, formaldehyde (HCHO) is one of the major species (Zhang et al., 2016). Long term exposure of lower concentration of formaldehyde could cause eye and throat irritation and chest tightness (Tasbihi et al., 2015). Various

https://doi.org/10.1016/j.arabjc.2020.04.002
1878-5352

studies (Ai et al., 2010; Kim et al., 2011; Sekiguchi et al., 2011; Fan et al., 2011; Wan et al., 2011) have presented high conversions of formaldehyde degradation as catalytic oxidation (Kim et al., 2011), high-frequency ultrasound combination with photocatalytic way (Sekiguchi et al., 2011), plasma-catalytic removal method (Fan et al., 2011) and direct circuit corona discharge plasma method (Wan et al., 2011). The photo degradation of HCHO, commonly uses TiO_2-photocatalytic material in industry. There are several advantages of TiO_2 material towards photocatalytic HCHO degradation (Liu et al., 2008); for example high resistant to photo-corrosion, environmentally clean and known to completely oxidize HCHO into CO_2 and H_2O (Liang et al., 2012; Wang et al., 2012; Fu et al., 2011; Zhu and Wu, 2015).

Dyes have adverse effects on human body as well as aquatic life. These are readily used in textile, printing, dyeing, and related industries which discharge the huge amount of dye-containing wastewater into the environment and generates hazards for human health (Iram et al., 2010; Zhu et al., 2012; Fisli et al., 2014). Very small amount of dye in huge water reduces the photosynthesis efficiency for aquatic life. Dyes are generally thermo and photo stable and possess high resistance to chemical; these qualities increase the serious concern of scientist toward the removal of dyes from the wastewater (Girgis et al., 2015). The various techniques have been applied for removal of dyes from wastewaters (flocculation, coagulation, precipitation, membrane filtration, and adsorption techniques). Among these adsorption method associated with nanoadsorbent widely useful for dyes removal (Kong and Gan, 2012; Deng et al., 2013; Zhang et al., 2014; Zhou et al., 2015; Afkhami et al., 2010). There are some examples about the adsorption application using various adsorbents in recent studies (Van Tran et al., 2019a, 2019b, 2018c, 2019d, 2019e, 2019f, 2019g, 2020). The conventional activated carbon and zeolites have poor adsorption capacity and low dye removal efficiency (Sharma and Lee, 2015, 2017a, 2017b, 2014; Sharma et al., 2010). Thus, improvement of novel nanomaterials having high adsorption ability is still crucial task for scientist (Dehghanian et al., 2016). Sodium 1-[1-hydro xynaothylazo]-6-nitro-2-napthol-4-sulfonate i.e. Eriochrome black T (EBT) is anionic azo dye. It is hazardous (carcinogenic) in case of skin contact and irritant on eye contact. EBT is used in complexometric titrations and for dyeing silk (Dutta et al., 2014; Jethave et al., 2018a, 2018b). In previous years our research group reported the receptor for sensing of ions from wastewater (Fegade et al., 2014a, 2014b, 2014c, 2014d, 2014e, 2015; Jethave and Fegade, 2018; Kondalkar et al., 2018). The current study explored the application of ZnAlONPs for photo-degradation of formaldehyde as well as adsorption of EBT.

2. Experimental

2.1. Materials and instrumentation

All the chemicals used in this work were of analytical grade and purchased from Merck, Germany. The MiliQ water (A Grade) was used in every stage of the study. The characterization done by FE-SEM (Bruker S-4800 at 15.0 kV), EDX (500 × 375 Magnitude: 40,000 × HV:15.0 kV), FTIR (Model: FT-IR Bruker) in the range of 500–4000 cm^{-1} and UV–Visible spectrophotometer (Shimadzu UV-1800) at 25 °C.

2.2. Formaldehyde degradation system

During this study, 200 mg of ZnAlONPs was positioned in reactor with volume of 0.7L. HCHO gas was passed from reactor to test the photo catalytic activity of ZnAlONPs in 18 W daylight lamp of intensity 8.8 $mWcm^{-2}$ and the remaining concentration of HCHO is calculated after fixed interval (Supplementary Fig. S1). The HCHO degradation rate was determined by Eq. (1):

$$\text{HCHO degradation rate}\,(\%) = (C_0 - C_e)/C_0 \times 100\% \quad (1)$$

where C_0 and C_e are the initial and final concentration of HCHO gas, respectively.

2.3. Batch adsorption experiment for EBT dye removal

Adsorption behavior of EBT was performed by varying experimental parameters. Optimization of adsorption method is done by varying doses (50–200 mg) of ZnAlONPs into the 50 ml solution of different doses of EBT (50–200 mg) in a 100 ml conical flask. The solution was shaken for 90 min on rotary shaker at 200 rpm. The adsorption of dye is calculated, the aliquot taken at time interval centrifuged at 2000 rpm for 3 min and the supernant solution is used for the measurement of concentration of EBT using spectrophotometer at 489 nm. The concentration of EBT decreased with time due to its adsorption on ZnAlONPs. The adsorption capacity (q_e) of nanoparticles for EBT dye was calculated by Eq. (2).

$$q_e = (Ci - Ce)V/m \quad (2)$$

where Ci = initial concentrations, *Ce* = equilibrium concentrations (mg/L), *m* = mass of the adsorbent (g) and V = volume (L).

2.4. Kinetic models, adsorption isotherms, separation factor and thermodynamic parameters equations

The pseudo–II–order kinetic model formula

$$t/q_t = 1/k_{ad}q_e^{\,2} + t/q_e \quad (3)$$

The general form of the Langmuir isotherm is:

$$q_e\alpha_L/K_L = K_LC_e/(1 + K_LC_e) \quad (4)$$

After linearization of the Langmuir isotherm, Eq. (4), we obtain

$$C_e/q_e = C_e\alpha_L/K_L + 1/K_L \quad (5)$$

The adsorbed EBT (mg/g) was calculated based on a mass balance equation:

$$q_e = V(C_o - C_e)/m \quad (6)$$

The Freundlich isotherm can be expressed as:

$$q_e = K_fC_e^{\,1/n} \quad (7)$$

where Ce = equilibrium concentration (mg/L), qe = amount adsorbed at equilibrium (mg/g), and K_f and 1/n = Freundlich constants

The linearized form of the Freundlich adsorption isotherm equation is as follows

$$\ln q_e = \ln K_f + \ln C_e/n \quad (8)$$

A separation factor as described by Fegade et al. (2014e) (R_L), is defined as:

$$R_L = 1/(1 + \alpha_LC_o) \quad (9)$$

where α_L = Langmuir coefficient and C_0 = initial dye concentration.

Thermodynamic parameters equation

$$\Delta G = -RT \ln K_L \quad (10)$$

where R = (8.314 J mol^{-1} K^{-1}), T = Temperature and K_L = Langmuir constant (L mol^{-1}).

3. Results and discussion

3.1. Fabrication of ZnAlONPs

ZnAlONPs were fabricated by co-precipitation method followed by heating with stirring (Jethave et al., 2017). Initially 0.75 mol of $ZnCl_2$ and 1.0 mol of $AlCl_3$ were poured into the 300 ml distilled water (DW). Then 50 ml of 1 M NaOH and 30 ml ammonia was added drop wise with constant stirring for two hr at 60 °C. The white precipitates were dried for 4 h and then crushed into powder and again heated in an oven at 400 °C for 4 hr for calcinations. Fig. 1 show FE-SEM images of ZnAlONPs. Fig. 1(a), shows that the synthesized material has nano flake character and image (b) shows the nano flake size upto 70–90 nm. EDX spectrum confirmed the presence of Zn, Al and O in nano flake having 20.81, 10.15 and 69.03%, respectively (Fig. 2). The chemical composition of ZnAlONPs was explored using FTIR analysis and the FTIR spectrum is shown in Fig. 3. The broad band at 3366 cm^{-1} is assigned to the O—H stretching vibrations of free water (Zawrah and El Kheshen, 2002; Kurien, 2010). The band at 1358 cm^{-1} corresponds to metal–alloy (Zn–Al) and bands at 774 and 687 cm^{-1} are attributed to Zn—O bonds while bands at 545 and 511 cm^{-1} show the presence of the Al—O vibration bands (Zawrah and El Kheshen, 2002; Kurien, 2010) (Fig. 3).

3.2. Photo-degradation of formaldehyde

The photocatalytic HCHO degradation system and its working are given in supplementary Fig. S1. The photo-degradation of HCHO was investigated quantitatively using TiO_2 (homemade), TiO_2 (P25) and $Zn_{0.3}Al_{0.4}O_{4.5}$ under 18 W daylight lamp irradiation and the results are shown in Fig. 4. The degradation rate was found to be 67, 76 and 89% for TiO_2 (homemade), TiO_2 (P25) and $Zn_{0.3}Al_{0.4}O_{4.5}$

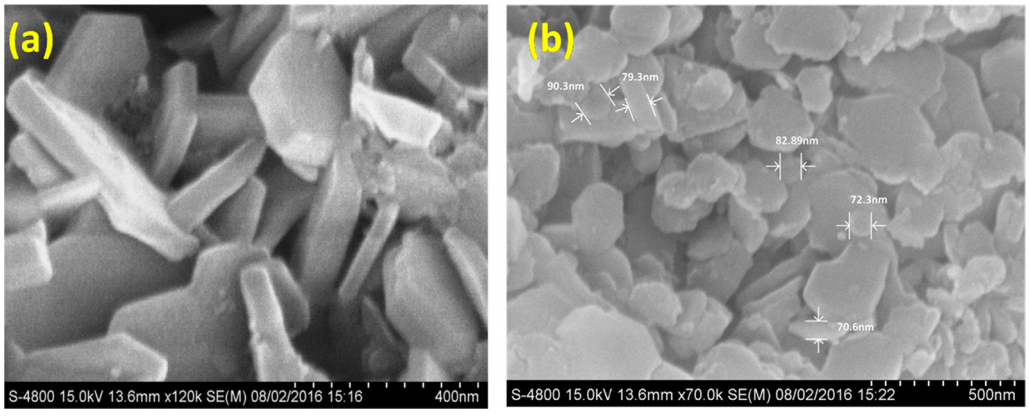

Fig. 1 (a) Closed FE-SEM image, and (b) FE-SEM images of nano flake ZnAlONPs with size 70–90 nm.

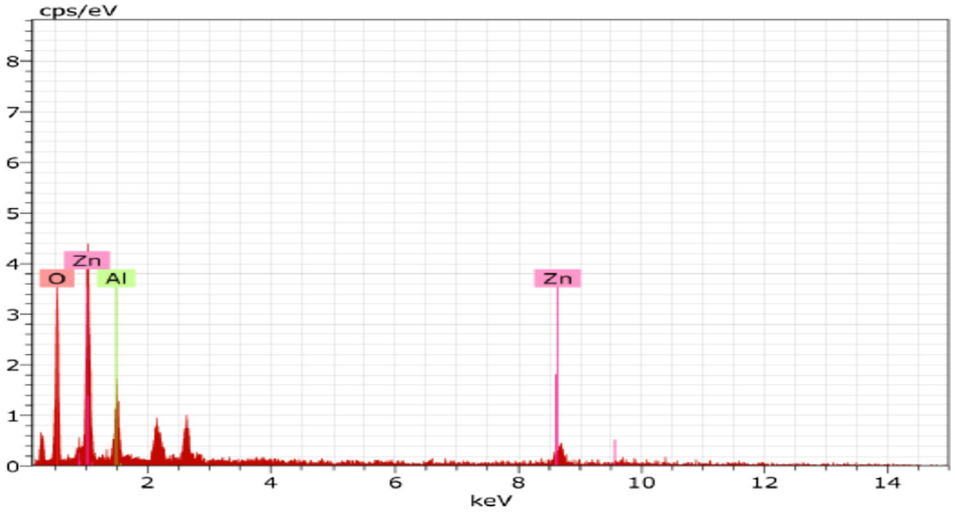

Fig. 2 EDX spectrum of the ZnAlONPs.

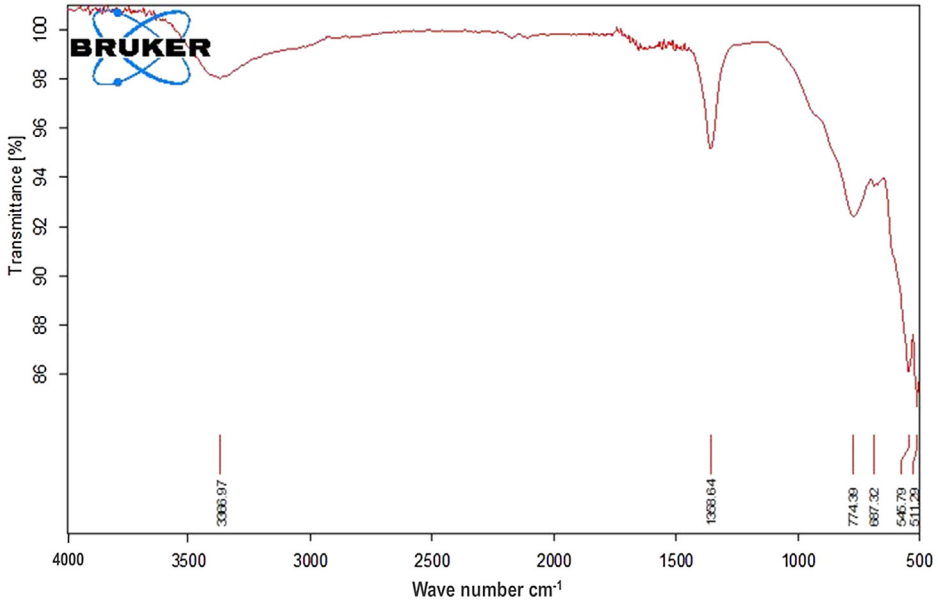

Fig. 3 FTIR spectrum of ZnAlONPs.

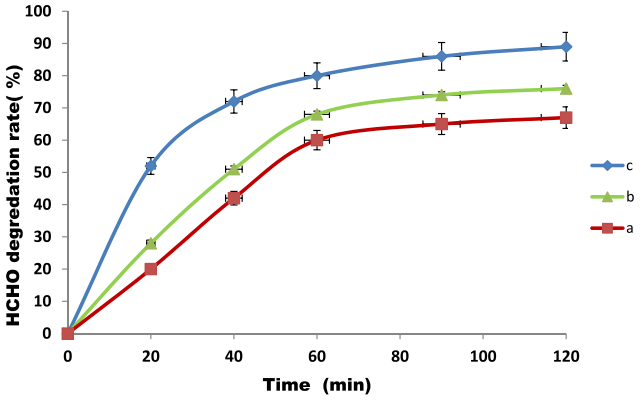

Fig. 4 The photo-degradation of 20 ppm HCHO by various photo-catalysts (a) Homemade TiO_2 (b) P-25 TiO_2 (c) ZnAlONPs under photo radiation.

during 2 h reaction, respectively (Supplimentry information Table S1). The ZnAlONPs showed a maximum photo-degradation efficiency for HCHO than other catalysts because ZnAlONPs have wide range and strong absorption in visible light region than the TiO_2 (P25).

3.3. Possible mechanism of HCHO degradation

HCHO photo-degradation mechanism as proposed is shown in Fig. 5 and Eqs. (11)–(16). Eq. (11) described the electron excitation and hole formation using photoenergy. Under visible light irradiation of ZnAlONPs the electrons present in valence band are excited and transfer to conduction band and form electron-hole pairs. The Eq. (13) shows the generation of •OH radicals using photocatalyst and Eqs. (14)–(16) shows the degradation of HCHO through the •OH radicals which is previously generated by photocatalyst in equation (13).

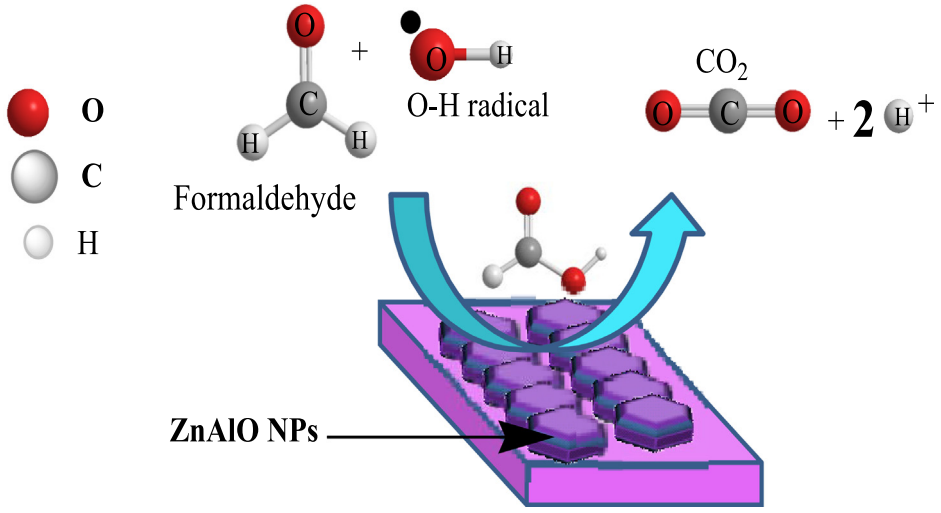

Fig. 5 Schematic representation of possible mechanism of HCHO degradation.

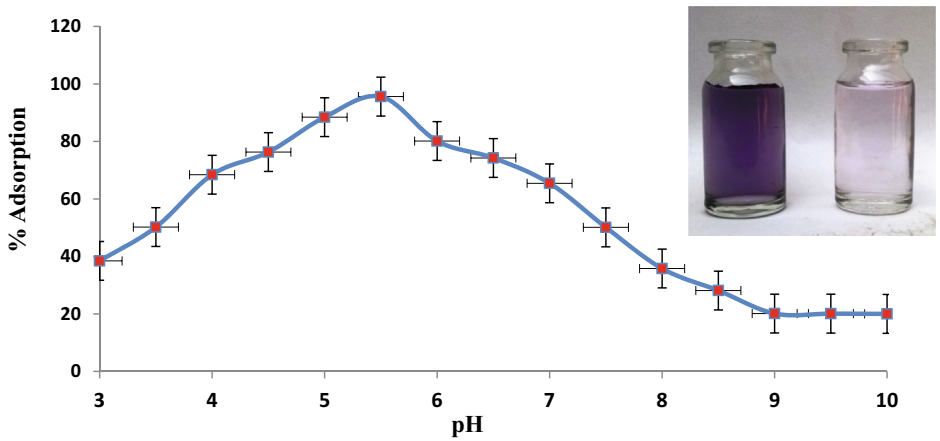

Fig. 6 Effect of pH on adsorption of EBT (conditions, ZnAlONPs dose = 200 mg, EBT concentration = 50 mg/L, shaking time = 90 min). Inset shows the color of dye solution before and after treatment.

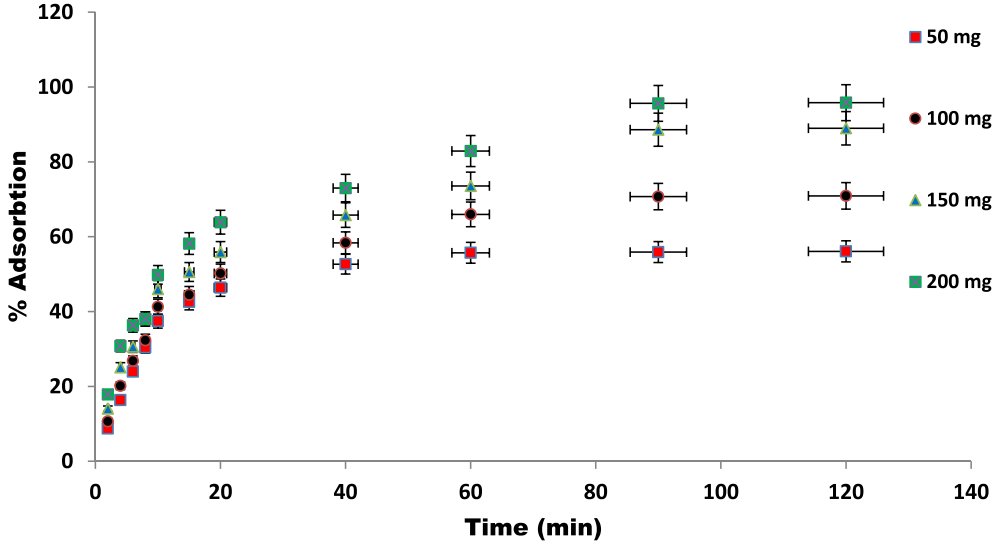

Fig. 7 Variation in ZnAlONPs dose at constant EBT concentration (at 25 °C).

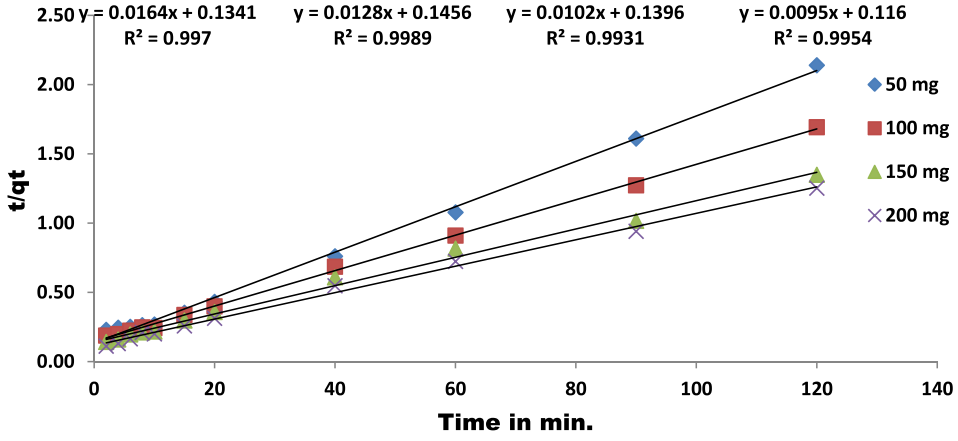

Fig. 8 Kinetic plots of EBT onto ZnAlONPs at various primary EBT concentrations.

Pl
(11)
H
(12)
h
(13)
H
(14)
H
(15)
H
(16)

Table 1 Result obtained by Kinetic equation.

Parameters				
Concentration (mg)	50	100	150	200
K_{ad} g mg^{-1} min^{-1}	0.045	0.094	0.089	0.083
qe (mg/g)	62.5	83.33	100	111.11
R^2	0.997	0.998	0.993	0.995

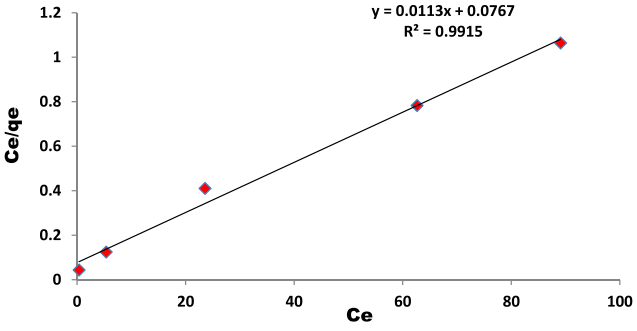

Fig. 9 Linearization of the Langmuir isotherm. Conditions: pH 5.5, and 25 °C.

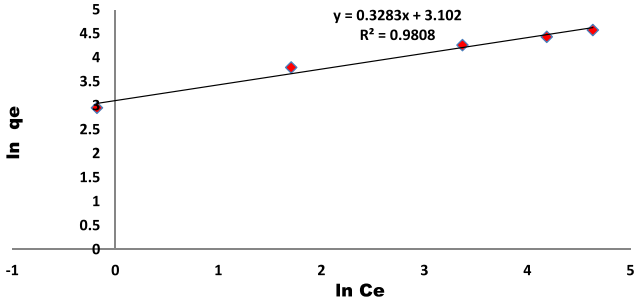

Fig. 10 Freundlich plot for the adsorption of EBT onto ZnAlONPs at 25 °C and pH 5.5.

3.4. Effect of pH, time and adsorbent variation

The effect of pH on dye adsorption using ZnAlONPs was evaluated at various pH ranges 3–10. Fig. 6 shows that percent adsorption enhance from 38 to 96% when the pH varies from 4 to 6. It is due to the protonation on ZnAlONPs. The dissociation constant pKa for EBT is 6.2 and 11.55, consequently EBT present as monovalent anions, at the equilibrium pH (Dehghanian et al., 2016). EBT was protonated and increases repulsion with ZnAlONPs due to similar charges and percent removal decreases at low pH. As demonstrated the experiment by varying the time from 0 to 120 min in supplementary Fig. S2, the maximum adsorption efficiency of EBT was achieved after 60 min and the phenomenon is explained based on that the great numbers of active sites if available but active sites required sufficient contact time for the chemical or physical interaction for adsorption. The influence of ZnAlONPs quantity on adsorption of EBT was examined in batch experiments by adding adsorbent in range of 50–200 mg in 50 mg L^{-1} dye solution. The results showed that the ZnAlONPs amount is directly proportional to percent adsorption, until it reaches a saturation point. The enhancement in percent adsorption with ZnAlONPs can be attributed to increased surface area and more adsorption sites. Fig. 7 results showed that the adsorption efficiencies (%) increased from 58.51 to 97.75% by increasing adsorbent dose from 50 to 200 mg due to availability of more adsorption sites.

3.5. Kinetic models, adsorption isotherms, separation factor and thermodynamic parameters

To determine the controlling mechanism of dye adsorption from aqueous solution, the adsorption kinetics of EBT on

Table 2 Data calculated from Langmuir and Freundlich.

Langmuir		Freundlich	
K_L	13.157	log K_f	1.347
$q_{max} = K_L/\alpha_L$	90.909	1/n	0.328
R^2	0.991	R^2	0.98

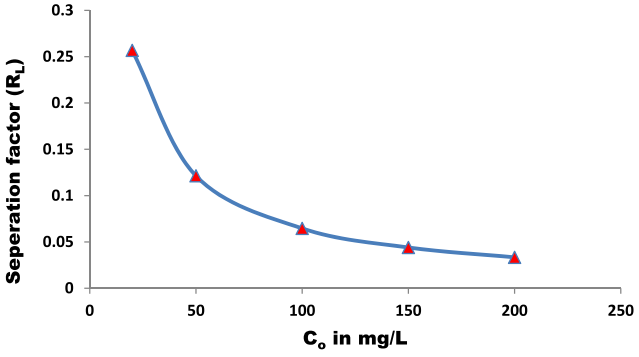

Fig. 11 R_L of the adsorption of EBT onto ZnAlONPs at 25 °C. (C_0 = initial EBT dye concentration).

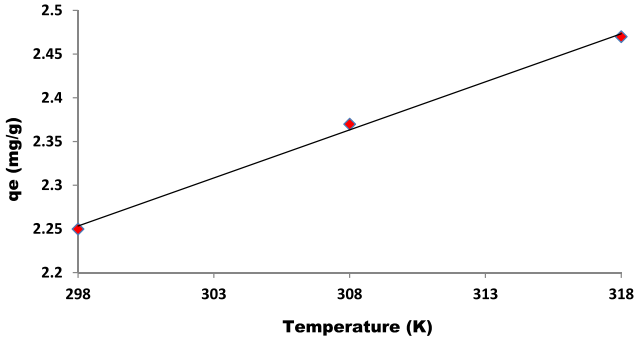

Fig. 12 Effect of temperature on qe of dye EBT using ZnAlONPs.

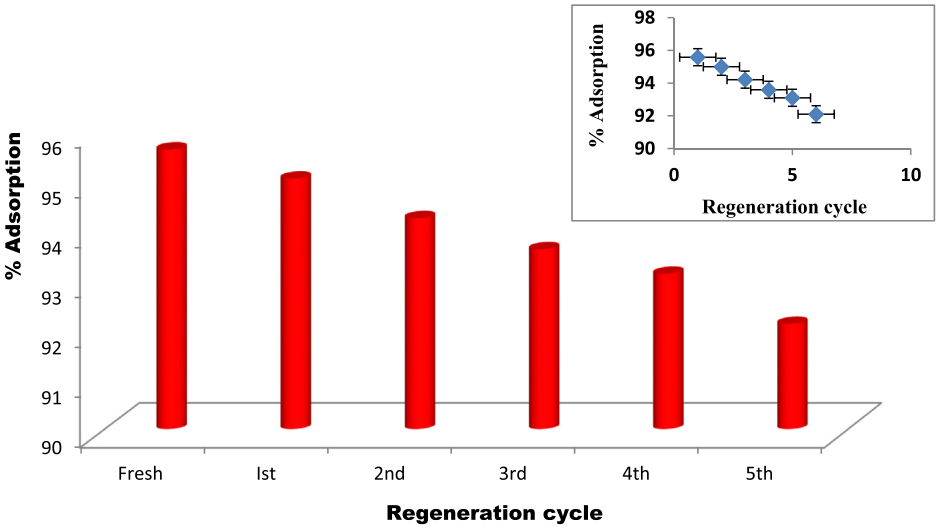

Fig. 13 Effect of reuse of ZnAlONPs by acid clean on adsorption.

ZnAlONPs was analyzed using kinetic models proposed by Ho and McKay (1999a, 1999b). The kinetic study confirmed the pseudo second-order (Fig. 8 and Table 1). The results obtained for adsorption of EBT were analyzed by the use of well known Langmuir (Dada, 2012; Langmuir, 1916, 1918) and Freundlich (Dada, 2012; Freundlich and Heller, 1939) models. The isotherms for EBT were obtained for ZnAlONPs at the solution pH of 5.5. The Figs. 9 and 10 represent the graph obtained by the adsorption isotherms and the calculated parameters are shown in Table 2. It is clear that the Langmuir is preeminent fitted than Freundlich of EBT adsorption. So, it is concluded that the above study may be a homogeneous monolayer adsorption. The separation factor (R_L) (Weber and Chakravorti, 1974) for EBT dye fall in between 0 and 1 which shows that dye adsorption on nano flake is a favorable adsorption process (Fig. 11). The study of temperature illustrated whether the process is exothermic or endothermic. The variation of dye EBT adsorbed on ZnAlONPs as function of solution temperature (Fegade et al., 2014a) is shown in Fig. 12. The ΔG determined is -7.08 kJ mol^{-1}. The negative ΔG specifies the spontaneous nature of process between adsorbent for the dyes (Banerjee and Chattopadhyaya, 2017; Deniz, 2013; Murcia-Salvador et al., 2019).

3.6. Reuse of ZnAlONPs by acidic cleaning

To explore the reuse ability of ZnAlONPs the dye adsorbed material converted in to desorbed material using HCl (0.1 M) and repeated upto five cycles. It is confirmed that the percent adsorption of ZnAlONPs is higher than 93% after the five reuse cycles (Fig. 13).

4. Conclusion

The ZnAlONPs showed the rapidest HCHO decomposition efficiency rate than TiO_2 catalysts. The ZnAlONPs synthesized by easy and economic way for EBT adsorption. The degradation of HCHO was studied on a variety of TiO_2 (home made), TiO_2 (P-25) and ZnAlONPs under photo irradiation. The HCHO degradation rate is about 67, 76 and 89% for TiO_2 (home made), TiO_2 (P25) and ZnAlONPs during 2 h reaction, respectively at 20 ppm initial formaldehyde concentration. The small amount 200 mg of the proposed ZnAlONPs is applicable for quick removal of EBT (> 95%). From the above results we can say that the synthesized nano flake will be the effective candidate for the HCHO photocatalysis as well as for EBT adsorption.

Acknowledgement

This project was funded by the Deanship of Scientific Research (DSR) at King Abdulaziz University, Jeddah, under grant no. KEP-54-130-38. The authors, therefore, acknowledge with thanks DSR for technical and financial support.

Appendix A. Supplementary material

Supplementary data to this article can be found online at https://doi.org/10.1016/j.arabjc.2020.04.002.

References

Afkhami, A., Saber-Tehrani, M., Bagheri, H., 2010. Modified maghemite nanoparticles as an efficient adsorbent for removing some cationic dyes from aqueous solution. Desalination 263, 240–248. https://doi.org/10.1016/j.desal.2010.06.065.

Ai, Z., Lee, S., Huang, Y., Ho, W., Zhang, L., 2010. Photocatalytic removal of NO and HCHO over nanocrystalline Zn_2SnO_4 microcubes for indoor air purification. J. Hazard. Mater. 179, 141–150. https://doi.org/10.1016/j.jhazmat.2010.02.071.

Banerjee, S., Chattopadhyaya, M.C., 2017. Adsorption characteristics for the removal of a toxic dye, tartrazine from aqueous solutions by a low cost agricultural by-product. Arab. J. Chem. 10, S1629–S1638. https://doi.org/10.1016/j.arabjc.2013.06.005.

Dada, A.O., 2012. Langmuir, Freundlich, Temkin and Dubinin-Radushkevich isotherms studies of equilibrium sorption of Zn^{2+} unto phosphoric acid modified rice husk. IOSR J. Appl. Chem. 3, 38–45. https://doi.org/10.9790/5736-0313845.

Dehghanian, N., Ghaedi, M., Ansari, A., Ghaedi, A., Vafaei, A., Asif, M., Agarwal, S., Tyagi, I., Gupta, V.K., 2016. A random forest approach for predicting the removal of Congo red from aqueous solutions by adsorption onto tin sulfide nanoparticles loaded on activated carbon. Desalin. Water Treat. 57, 9272–9285. https://doi.org/10.1080/19443994.2015.1027964.

Deng, J.H., Zhang, X.R., Zeng, G.M., Gong, J.L., Niu, Q.Y., Liang, J., 2013. Simultaneous removal of Cd(II) and ionic dyes from aqueous solution using magnetic graphene oxide nanocomposite as an adsorbent. Chem. Eng. J. 226, 189–200. https://doi.org/10.1016/j.cej.2013.04.045.

Deniz, F., 2013. Adsorption properties of low-cost biomaterial derived from Prunus amygdalus L. for dye removal from water. Sci. World J. 9. https://doi.org/10.1155/2013/961671.

Dutta, D.P., Singh, A., Ballal, A., Tyagi, A.K., 2014. High adsorption capacity for cationic dye removal and antibacterial properties of sonochemically synthesized Ag_2WO_4 nanorods. Eur. J. Inorg. Chem. 2014, 5724–5732. https://doi.org/10.1002/ejic.201402612.

Fan, X., Zhu, T., Sun, Y., Yan, X., 2011. The roles of various plasma species in the plasma and plasma-catalytic removal of low-concentration formaldehyde in air. J. Hazard. Mater. 196, 380–385. https://doi.org/10.1016/j.jhazmat.2011.09.044.

Fegade, U.A., Sahoo, S.K., Singh, A., Singh, N., Attarde, S.B., Kuwar, A.S., 2015. A chemosensor showing discriminating fluorescent response for highly selective and nanomolar detection of Cu^{2+} and Zn^{2+} and its application in molecular logic gate. Anal. Chim. Acta. 872, 63–69. https://doi.org/10.1016/j.aca.2015.02.051.

Fegade, U., Sahoo, S.K., Attarde, S., Singh, N., Kuwar, A., 2014a. Colorimetric and fluorescent "on-off" chemosensor for Cu^{2+} in semi-aqueous medium. Sensors Actuators, B Chem. 202, 924–928. https://doi.org/10.1016/j.snb.2014.06.033.

Fegade, U., Sharma, H., Bondhopadhyay, B., Basu, A., Attarde, S., Singh, N., Kuwar, A., 2014b. "Turn-on" fluorescent dipodal chemosensor for nano-molar detection of Zn^{2+}: application in living cells imaging. Talanta 125, 418–424. https://doi.org/10.1016/j.talanta.2014.03.002.

Fegade, U., Sahoo, S.K., Singh, A., Mahulikar, P., Attarde, S., Singh, N., Kuwar, A., 2014c. A selective and discriminating noncyclic receptor for HSO_4^- ion recognition. RSC Adv. 4, 15288–15292. https://doi.org/10.1039/c3ra47935h.

Fegade, U., Singh, A., Chaitanya, G.K., Singh, N., Attarde, S., Kuwar, A., 2014d. Highly selective and sensitive receptor for Fe^{3+} probing. Spectrochim. Acta - Part A Mol. Biomol. Spectrosc. 121, 569–574. https://doi.org/10.1016/j.saa.2013.11.007.

Fegade, U., Tayade, S., Chaitanya, G.K., Attarde, S., Kuwar, A., 2014e. Fluorescent and chromogenic receptor bearing amine and hydroxyl functionality for iron (III) detection in aqueous solution. J. Fluoresc. 24, 675–681. https://doi.org/10.1007/s10895-014-1358-3.

Fisli, A., Yusuf, S., Krisnandi, Y.K., Gunlazuardi, J., 2014. Preparation and characterization of magnetite-silica nano-composite as adsorbents for removal of methylene blue dyes from environmental water samples. In: Adv. Mater. Res., Trans Tech Publ, 2014, pp. 525–531.

Freundlich, H., Heller, W., 1939. The adsorption of cis- and trans-Azobenzene. J. Am. Chem. Soc. 61, 2228–2230. https://doi.org/10.1021/ja01877a071.

Fu, P., Zhang, P., Li, J., 2011. Photocatalytic degradation of low concentration formaldehyde and simultaneous elimination of ozone by-product using palladium modified TiO_2 films under UV254 +185 nm irradiation. Appl. Catal. B Environ. 105, 220–228. https://doi.org/10.1016/j.apcatb.2011.04.021.

Girgis, E., Adel, D., Tharwat, C., Attallah, O., Rao, K.V., 2015. Cobalt ferrite nanotubes and porous nanorods for dye removal. Adv. Nano Res. 3, 111–121. https://doi.org/10.12989/anr.2015.3.2.111.

Ho, Y.S., McKay, G., 1999a. Pseudo-second order model for sorption processes. Process Biochem. 34, 451–465. https://doi.org/10.1016/S0032-9592(98)00112-5.

Ho, Y.S., McKay, G., 1999b. Comparative sorption kinetic studies of dye and aromatic compounds onto fly ash. J. Environ. Sci. Heal. - Part A Toxic./Hazard. Subst. Environ. Eng. 34, 1179–1204. https://doi.org/10.1080/10934529909376889.

Iram, M., Guo, C., Guan, Y., Ishfaq, A., Liu, H., 2010. Adsorption and magnetic removal of neutral red dye from aqueous solution using Fe_3O_4 hollow nanospheres. J. Hazard. Mater. 181, 1039–1050. https://doi.org/10.1016/j.jhazmat.2010.05.119.

Jethave, G., Fegade, U., Attarde, S., Ingle, S., 2017. Facile synthesis of lead doped zinc-aluminum oxide nanoparticles (LD-ZAO-NPs) for efficient adsorption of anionic dye: Kinetic, isotherm and thermodynamic behaviors. J. Ind. Eng. Chem. 53. https://doi.org/10.1016/j.jiec.2017.04.038.

Jethave, G., Fegade, U., 2018. Design and synthesis of $Zn_{0.3}Fe_{0.45}O_3$ nanoparticle for efficient removal of Congo red dye and its kinetic and isotherm investigation. Int. J. Ind. Chem. 9, 85–97. https://doi.org/10.1007/s40090-018-0140-9.

Jethave, G., Su, K., Huang, W., Wu, R., Jethave, G., Su, K., Huang, W., Wu, R., 2018a. An multifunction $Zn_{0.3}Mn_{0.4}O_4$ nanospheres for carbon dioxide reduction to methane via photocatalysis and reused after fifth cycles for phosphate adsorption. J. Environ Chem. Eng.

Jethave, G., Fegade, U., Rathod, R., Pawar, J., 2018b. Dye pollutants removal from waste water using metal oxide nanoparticle embedded activated carbon: an immobilization study. J. Dispers. Sci. Technol. 40, 563–573. https://doi.org/10.1080/01932691.2018.1472016.

Kim, S.S., Park, K.H., Hong, S.C., 2011. A study on HCHO oxidation characteristics at room temperature using a Pt/TiO_2 catalyst. Appl. Catal. A Gen. 398, 96–103. https://doi.org/10.1016/j.apcata.2011.03.018.

Kondalkar, M., Fegade, U., Attarde, S., Ingle, S., 2018. Experimental investigation on phosphate adsorption, mechanism and desorption properties of Mn-Zn-Ti oxide trimetal alloy nanocomposite. J. Dispers. Sci. Technol. 39, 1635–1643. https://doi.org/10.1080/01932691.2018.1459678.

Kong, L.P., Gan, X.J., Bin Ahmad, A.L., Hamed, B.H., Evarts, E.R., Ooi, B.S., Lim, J.K., 2012. Design and synthesis of magnetic nanoparticles augmented microcapsule with catalytic and magnetic bifunctionalities for dye removal. Chem. Eng. J. 197, 350–358. https://doi.org/10.1016/j.cej.2012.05.019.

Kurien, S., 2010. Analysis of FTIR spectra of nanoparticles of $MgAl_2O_4$, $SrAl_2O_4$, and $NiAl_2O_4$. http://shodhganga.inflibnet.ac.in:8080/jspui/bitstream/10603/468/10/10_chapter4.pdf.

Langmuir, I., 1916. The constitution and fundamental properties of solids and liquids. Part I. Solids. J. Am. Chem. Soc. 38, 2221–2295. https://doi.org/10.1021/ja02268a002.

Langmuir, I., 1918. The adsorption of gases on plane surfaces of glass, mica and platinum. J. Am. Chem. Soc. 40, 1361–1403. https://doi.org/10.1021/ja02242a004.

Liang, W., Li, J., Jin, Y., 2012. Photo-catalytic degradation of gaseous formaldehyde by TiO_2/UV, Ag/TiO_2/UV and Ce/TiO_2/UV. Build. Environ. 51, 345–350. https://doi.org/10.1016/j.buildenv.2011.12.007.

Liu, T.X., Li, F.B., Li, X.Z., 2008. TiO_2 hydrosols with high activity for photocatalytic degradation of formaldehyde in a gaseous phase. J. Hazard. Mater. 152, 347–355. https://doi.org/10.1016/j.jhazmat.2007.07.003.

Murcia-Salvador, A., Pellicer, J.A., Fortea, M.I., Gómez-López, V. M., Rodríguez-López, M.I., Núñez-Delicado, E., Gabaldón, J.A., 2019. Adsorption of Direct Blue 78 using chitosan and cyclodextrins as adsorbents. Polymers (Basel) 11. https://doi.org/10.3390/polym11061003.

Sekiguchi, K., Sasaki, C., Sakamoto, K., 2011. Synergistic effects of high-frequency ultrasound on photocatalytic degradation of aldehydes and their intermediates using TiO_2 suspension in water. Ultrason. Sonochem. 18, 158–163. https://doi.org/10.1016/j.ultsonch.2010.04.008.

Sharma, A., Lee, B.K., 2014. Cd(II) removal and recovery enhancement by using acrylamide-titanium nanocomposite as an adsorbent. Appl. Surf. Sci. 313, 624–632. https://doi.org/10.1016/j.apsusc.2014.06.034.

Sharma, A., Lee, B.K., 2015. Synthesis and characterization of anionic/nonionic surfactant-interceded iron-doped TiO_2 to enhance sorbent/photo-catalytic properties. J. Solid State Chem. 229, 1–9. https://doi.org/10.1016/j.jssc.2015.04.042.

Sharma, A., Lee, B.K., 2017a. Growth of TiO_2 nano-wall on activated carbon fibers for enhancing the photocatalytic oxidation of benzene in aqueous phase. Catal. Today. 287, 113–121. https://doi.org/10.1016/j.cattod.2016.11.019.

Sharma, A., Lee, B.K., 2017b. Photocatalytic reduction of carbon dioxide to methanol using nickel-loaded TiO_2 supported on activated carbon fiber. Catal. Today 298, 158–167. https://doi.org/10.1016/j.cattod.2017.05.003.

Sharma, A., Verma, N., Sharma, A., Deva, D., Sankararamakrishnan, N., 2010. Iron doped phenolic resin based activated carbon micro and nanoparticles by milling: synthesis, characterization and application in arsenic removal. Chem. Eng. Sci. 65, 3591–3601. https://doi.org/10.1016/j.ces.2010.02.052.

Tasbihi, M., Bendyna, J.K., Notten, P.H.L., Hintzen, H.T., 2015. A short review on photocatalytic degradation of formaldehyde. J. Nanosci. Nanotechnol. 15, 6386–6396. https://doi.org/10.1166/jnn.2015.10872.

Van Tran, T., Nguyen, D.T.C., Le, H.T.N., Nguyen, O.T.K., Nguyen, V.H., Nguyen, T.T., Bach, L.G., Nguyen, T.D., 2019a. A hollow mesoporous carbon from metal-organic framework for robust adsorbability of ibuprofen drug in water. R. Soc. Open Sci. 6. https://doi.org/10.1098/rsos.190058.

Van Tran, T., Nguyen, D.T.C., Le, H.T.N., Bach, L.G., Vo, D.-V.N., Lim, K.T., Nong, L.X., Nguyen, T.D., 2019b. Combined minimum-run resolution IV and central composite design for optimized removal of the tetracycline drug over metal-organic framework-templated porous carbon. Molecules 24, 1887. https://doi.org/10.3390/molecules24101887.

Van Tran, T., Nguyen, D.T.C., Le, H.T.N., Duong, C.D., Bach, L.G., Nguyen, H.T.T., Nguyen, T.D., 2019c. Facile synthesis of manganese oxide-embedded mesoporous carbons and their adsorbability towards methylene blue. Chemosphere 227, 455–461. https://doi.org/10.1016/j.chemosphere.2019.04.079.

Van Tran, T., Cao, V.D., Nguyen, V.H., Hoang, B.N., Vo, D.V.N., Nguyen, T.D., Bach, L.G., 2019d. MIL-53 (Fe) derived magnetic porous carbon as a robust adsorbent for the removal of phenolic compounds under the optimized conditions. J. Environ. Chem. Eng. 8,. https://doi.org/10.1016/j.jece.2019.102902 102902.

Van Tran, T., Nguyen, D.T.C., Le, H.T.N., Bach, L.G., Vo, D.V.N., Dao, T.U.T., Lim, K.T., Nguyen, T.D., 2019e. Effect of thermolysis condition on characteristics and nonsteroidal anti-inflammatory drugs (NSAIDs) absorbability of Fe-MIL-88B-derived mesoporous carbons. J. Environ. Chem. Eng. 7,. https://doi.org/10.1016/j.jece.2019.103356 103356.

Van Tran, T., Nguyen, D.T.C., Nguyen, H.T.T., Nanda, S., Vo, D.V.N., Do, S.T., Van Nguyen, T., Thi, T.A.D., Bach, L.G., Nguyen, T. D., 2019f. Application of Fe-based metal-organic framework and its pyrolysis products for sulfonamide treatment. Environ. Sci. Pollut. Res. 26, 28106–28126. https://doi.org/10.1007/s11356-019-06011-2.

Van Tran, T., Nguyen, D.T.C., Le, H.T.N., Bach, L.G., Vo, D.V.N., Hong, S.S., Phan, T.Q.T., Nguyen, T.D., 2019g. Tunable synthesis of mesoporous carbons from $Fe_3O(BDC)_3$ for chloramphenicol antibiotic remediation. Nanomaterials 9, 237. https://doi.org/10.3390/nano9020237.

Van Tran, T., Nguyen, D.T.C., Le, H.T.N., Vo, D.-V.N., Nanda, S., Nguyen, T.D., 2020. Optimization, equilibrium, adsorption behavior and role of surface functional groups on graphene oxide-based nanocomposite towards diclofenac drug. J. Environ. Sci. https://doi.org/10.1016/j.jes.2020.02.007.

Wan, Y., Fan, X., Zhu, T., 2011. Removal of low-concentration formaldehyde in air by DC corona discharge plasma. Chem. Eng. J. 171, 314–319. https://doi.org/10.1016/j.cej.2011.04.011.

Wang, J., Liu, X., Li, R., Qiao, P., Xiao, L., Fan, J., 2012. TiO_2 nanoparticles with increased surface hydroxyl groups and their improved photocatalytic activity. Catal. Commun. 19, 96–99. https://doi.org/10.1016/j.catcom.2011.12.028.

Weber, T.W., Chakravorti, R.K., 1974. Pore and solid diffusion models for fixed-bed adsorbers. AIChE J. 20, 228–238. https://doi.org/10.1002/aic.690200204.

Zawrah, M.F.M., El Kheshen, A.A., 2002. Synthesis and characterisation of nanocrystalline $MgAl_2O_4$ ceramic powders by use of molten salts. Br. Ceram. Trans. 101, 71–74. https://doi.org/10.1179/096797801225000888.

Zhang, Y.-R., Shen, S.-L., Wang, S.-Q., Huang, J., Su, P., Wang, Q.-R., Zhao, B.-X., 2014. A dual function magnetic nanomaterial modified with lysine for removal of organic dyes from water solution. Chem. Eng. J. 239, 250–256.

Zhang, W., Song, N., Guan, L., Li, F., Yao, M., 2016. Photocatalytic degradation of formaldehyde by nanostructured TiO_2 composite films. J. Exp. Nanosci. 11, 185–196. https://doi.org/10.1080/17458080.2015.1043657.

Zhou, Q., Gao, Q., Luo, W., Yan, C., Ji, Z., Duan, P., 2015. One-step synthesis of amino-functionalized attapulgite clay nanoparticles adsorbent by hydrothermal carbonization of chitosan for removal of methylene blue from wastewater. Colloids Surf. A Physicochem. Eng. Asp. 470, 248–257. https://doi.org/10.1016/j.colsurfa.2015.01.092.

Zhu, T., Chen, J.S., Lou, X.W.D., 2012. Highly efficient removal of organic dyes from waste water using hierarchical NiO spheres with high surface area. J. Phys. Chem. C 116, 6873–6878. https://doi.org/10.1021/jp300224s.

Zhu, Z., Wu, R.J., 2015. The degradation of formaldehyde using a $Pt@TiO_2$ nanoparticles in presence of visible light irradiation at room temperature. J. Taiwan Inst. Chem. Eng. 50, 276–281. https://doi.org/10.1016/j.jtice.2014.12.022.